C. R. Physique 19 (2018) 43–53

Contents lists available at ScienceDirect

Comptes Rendus Physique

www.sciencedirect.com

Radio science for Humanity / Radiosciences au service de l'humanité

The double Brewster angle effect

Le double effet de Brewster

Laetitia Thirion-Lefevre *, Régis Guinvarc'h

CentraleSupélec, SONDRA, Plateau de Moulon, 3, rue Joliot-Curie, 91192 Gif-sur-Yvette cedex, France

ARTICLE INFO

Article history:
Available online 15 February 2018

Keywords:
RADAR
Polarization
Double bounces
Brewster angle
Urban areas
Forests

Mots-clés :
RADAR
Polarisation
Double rebond
Angle de Brewster
Zones urbaines
Forêts

ABSTRACT

The Double Brewster angle effect (DBE) is an extension of the Brewster angle to double reflection on two orthogonal dielectric surfaces. It results from the combination of two pseudo-Brewster angles occurring in complementary incidence angles domains. It can be observed for a large range of incidence angles provided that double bounces mechanism is present. As a consequence of this effect, we show that the reflection coefficient at VV polarization can be at least 10 dB lower than the reflection coefficient at HH polarization over a wide range of incidence angle – typically from 20 to 70°. It is experimentally demonstrated using a Synthetic Aperture Radar (SAR) image that this effect can be seen on buildings and forests. For large buildings, the difference can reach more than 20 dB.

RÉSUMÉ

Le double effet de Brewster (DEB) est une extension de l'effet induit par l'angle de Brewster au cas d'une double réflexion sur deux surfaces diélectriques orthogonales. Il en résulte alors deux pseudo-angles de Brewster se produisant dans des domaines angulaires complémentaires. La combinaison de ces deux mécanismes implique que cet effet peut être observé pour une grande gamme d'angles d'incidence, à condition que le mécanisme de double rebond soit présent. La conséquence remarquable est que le coefficient de rétrodiffusion en polarisation VV peut être inférieur d'au moins 10 dB par rapport au coefficient de réflexion en polarisation HH, et ceci sur une large gamme d'angle d'incidence – typiquement de 20 à 70°. Nous proposons une vérification de cet effet en utilisant une image radar à synthèse d'ouverture (RSO). Pour les grands bâtiments, la différence peut atteindre plus de 20 dB ; il est également observable, dans une moindre mesure cependant, pour la lisière d'une forêt.

* Corresponding author.
E-mail addresses: laetitia.thirion@centralesupelec.fr (L. Thirion-Lefevre), regis.guinvarch@centralesupelec.fr (R. Guinvarc'h).

https://doi.org/10.1016/j.crhy.2018.02.003

1. Introduction

When an electromagnetic wave is incident on a planar and horizontal interface between two dielectrics, a transmitted wave and a reflected wave are generated. When there are no losses within the materials, only the parallel component of the reflected wave exists for a specific angle, called the polarizing angle. This angle is bounded and can go from 45° to 90°, depending on permittivity. This effect was discovered more than two hundred years ago by Brewster [1]. When the incident wave is unpolarized, as for light, this effect could be used to polarize it. When the incident wave is polarized, as for radio waves, it acts as a polarization filter. Whatever the polarization state of the incident wave, this effect occurs for a narrow range of incidence angle, as seen in Fig. 2. In order to account for the losses of materials, the pseudo-Brewster angle has been introduced [2]. At this angle, the reflected intensity for the perpendicular component is no longer zero, but a minimum. Thus, the perpendicular component exists, but it may be strongly attenuated. In addition, this effect is then larger in angular range, as illustrated in Fig. 3.

The specular configuration is typically used in optics to retrieve the optical constants of the complex refractive index, which is the square root of the complex relative permittivity. However, for classical radar systems, the transmitter and the receiver are generally located next to each other, so the specular configuration on a single interface is not of prime interest. Now, if we combine two orthogonal interfaces, then a strong signal can be scattered back to the radar. This implies cascading two pseudo-Brewster angles: one that may range from 45° to 90° (horizontal interface) and the other from 0° to 45° (vertical interface). The combination of two nulls (Brewster effect) or two minimums (pseudo-Brewster effect) enlarges a lot the angular domain where there is a strong difference between parallel and perpendicular components. In what follows, we will refer to this phenomenon as the double Brewster angle effect, and it will be noted DBE.

In this paper, it is demonstrated both theoretically and experimentally that this double Brewster angle effect can be potentially observed in any monostatic radar images of the earth land surface. Indeed, by cascading two Brewster effects on two orthogonal surfaces, we obtain an effect that is observable for most of radar remote sensing configurations in terms of frequency and incidence angle. In addition, this effect exists for a wide angular range for a large variety of materials. We experimentally validate this effect on two radar images at different frequencies, and for two platforms – airborne and space borne – leading to various incidence angles and resolutions. Most of current space borne radar missions are concerned (RS2, TX, ALOS-PALSAR, Sentinel 1, etc.), as well as radar mounted on aircrafts by research agencies (SETHI, UAVSAR, E-SAR, CARABAS, etc.) as they all operate at incidence angles that may be affected by DBE. Consequently, we expect to observe this effect on a wide range of products delivered by these sensors.

In the next section, we recall the definitions of the Brewster and the pseudo- Brewster angles. In section 3, we introduce the double Brewster angle effect and show how sensitive it is to permittivity. Then in section 4, these results are illustrated and validated using real radar data, with a mixed landscape of urban and vegetated areas.

2. What are the Brewster and the pseudo-Brewster angles?

2.1. The polarizing angle of Sir David Brewster

Two hundred years ago, in March 1815, Sir David Brewster published his experimental results on the polarization of light [1]. His work actually extended the discovery of Étienne-Louis Malus, a French engineer, mathematician, and physicist who brought out the way to polarize the light using reflection on several materials. Sir David Brewster empirically determined that, for a specific angle – called the polarizing angle – "the reflected light is linearly polarized, but the transmitted light has both parallel- and perpendicularly-polarized components." [3] As Fresnel published his work later, in 1822 [4], Brewster could not express his observations in terms of reflection coefficients. The definition of this polarizing angle has evolved since then, and what we call now the Brewster angle is widely taught as the angle leading to a zero reflection coefficient for VV polarization, when transmission and reception are vertically polarized. As pointed out in [3], these two quantities (polarizing angle and zero reflection angle) are actually equal, provided that the experiment deals with "dielectric-dielectric interfaces". We investigate here the interfaces between air and either natural (wood, soil, etc.) or artificial (concrete, glass, etc.) materials. For these types of interface, provided that there is no loss, it is correct to define the Brewster angle as "a zero reflection coefficient" at VV polarization.

In Fig. 1, we consider an infinitely long interface between two media m_1 and m_2, characterized by their real relative permittivities ε_{r1} and ε_{r2}. For simplicity, we assume that m_1 is the air, so that $\varepsilon_{r1} = 1$, and the relative permeability of the two media is constant and equal to 1. We recall here that the permittivity may vary with frequency, temperature, moisture, and other contents of the material (see for instance [5] or [6]). For any incidence angle θ, we can determine the part of the incident field that is reflected in the specular direction using the Fresnel reflection coefficients R_v and R_h written as:

$$R_\mathrm{v}(\theta) = \frac{\varepsilon_{r2}\cos\theta - \sqrt{\varepsilon_{r2} - \sin^2\theta}}{\varepsilon_{r2}\cos\theta + \sqrt{\varepsilon_{r2} - \sin^2\theta}} \tag{1}$$

$$R_\mathrm{h}(\theta) = \frac{\cos\theta - \sqrt{\varepsilon_{r2} - \sin^2\theta}}{\cos\theta + \sqrt{\varepsilon_{r2} - \sin^2\theta}} \tag{2}$$

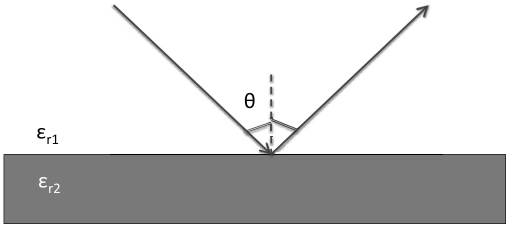

Fig. 1. The specular scattering is represented with the incidence angle θ; it occurs over the interface between two media characterized by their relative permittivities ε_{r1} and ε_{r2}.

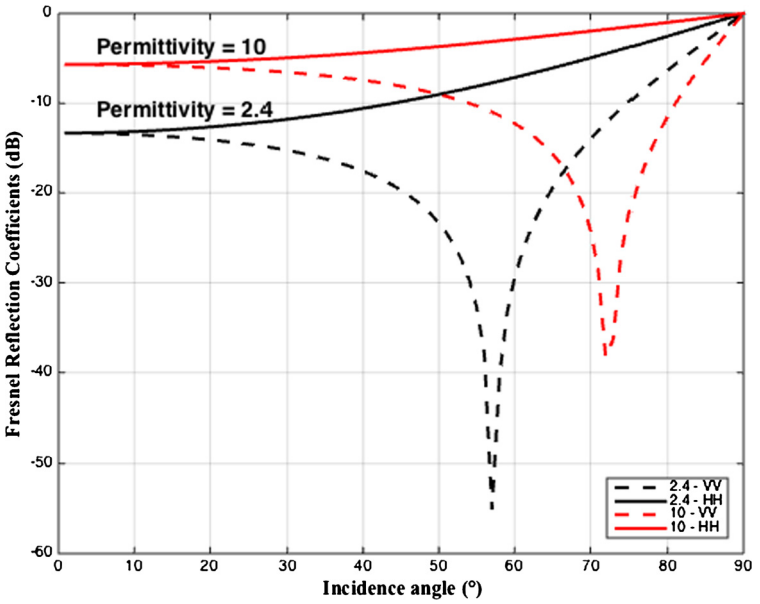

Fig. 2. The reflection coefficients are plotted in plain lines for $10\log_{10}\left(|R_{\mathrm{h}}|^2\right)$ and in dashed lines for $10\log_{10}\left(|R_{\mathrm{v}}|^2\right)$. The case ($\varepsilon_{r2} = 10$) is plotted in red, while the case ($\varepsilon_{r2} = 2.4$) appears in black.

At the Brewster angle θ_{B}, the incident field is totally transmitted for vertical (V) polarization, so that R_{v} reaches a null. The angle θ_{B} can be analytically determined using the Snell–Descartes law at the Brewster angle, and we obtain (see for instance [7] for a recall of the demonstration):

$$\theta_{\mathrm{B}} = \arctan\sqrt{\varepsilon_{r2}} \tag{3}$$

The Brewster angle in Eq. (3) is actually defined for a dielectric without any loss (ε_{r2} is real) and as $\varepsilon_{r2} \geq 1$, this angle is bounded, so that:

$$90^\circ \geq \theta_{\mathrm{B}} \geq 45^\circ \tag{4}$$

It is to be noted that the horizontal (H) polarized wave is not affected by this phenomenon.

Fig. 2 shows these Fresnel reflection coefficients as a function of the incidence angle θ for an interface between the air and two dielectrics for m_2: either $\varepsilon_{r2} = 2.4$ (in black) or $\varepsilon_{r2} = 10$ (in red). These values correspond to real parts of bitumen and concrete at 600 MHz. The square absolute value of the reflection coefficients are plotted in plain lines for R_{h} and in dashed lines for R_{v}. In Fig. 2, we can notice the first Brewster angle at 57.2 (corresponding to $\varepsilon_{r2} = 2.4$). When we turn to $\varepsilon_{r2} = 10$ (dashed red curve), we can see the Brewster angle at $\theta_{\mathrm{B}} = 72.5$ degrees.

2.2. The pseudo-Brewster angle

The Fresnel equations can be directly applied with complex relative permittivity with $\varepsilon_{\mathrm{r2}} = \varepsilon'_{\mathrm{r2}} - \mathrm{j}\varepsilon''_{\mathrm{r2}}$, and $\varepsilon'_{\mathrm{r2}}$ and $\varepsilon''_{\mathrm{r2}}$ its real and imaginary parts. We can still write:

$$R_{\mathrm{v}}(\theta) = \frac{\varepsilon_{\mathrm{r2}}\cos\theta - \sqrt{\varepsilon_{\mathrm{r2}} - \sin^2\theta}}{\varepsilon_{\mathrm{r2}}\cos\theta + \sqrt{\varepsilon_{\mathrm{r2}} - \sin^2\theta}} \tag{5}$$

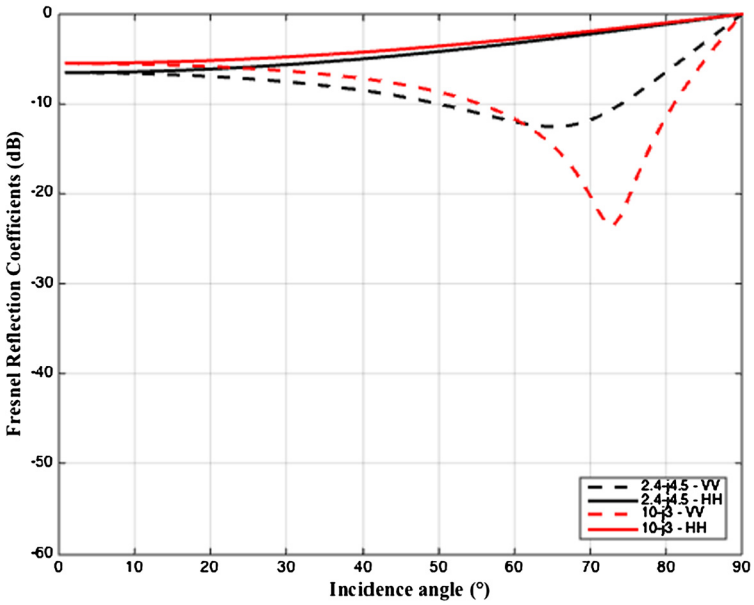

Fig. 3. The reflection coefficients are plotted in plain lines for $10\log_{10}\left(|R_{\mathrm{h}}|^2\right)$ and in dashed lines for $10\log_{10}\left(|R_{\mathrm{v}}|^2\right)$. The case $(\varepsilon_{\mathrm{r}2} = 10 - \mathrm{j}\,3)$ is plotted in red, while the case $(\varepsilon_{\mathrm{r}2} = 2.4 - \mathrm{j}\,4.5)$ appears in black.

$$R_{\mathrm{h}}(\theta) = \frac{\cos\theta - \sqrt{\varepsilon_{\mathrm{r}2} - \sin^2\theta}}{\cos\theta + \sqrt{\varepsilon_{\mathrm{r}2} - \sin^2\theta}} \tag{6}$$

In Fig. 3, we consider two complex permittivities (bitumen and concrete at 600 MHz): $\varepsilon_{r_2} = 2.4 - \mathrm{j}\,4.5$ (in black) or $\varepsilon_{r_2} = 10 - \mathrm{j}\,3$ (in red). We observe similar effect as in Fig. 2: R_{v} can be significantly lower than R_{h} (up to 10 dB in this example). The shape of R_{v} depends on the permittivity of the medium.

The imaginary part has thus several effects: first, the Brewster angle is shifted towards higher values, and the reflection coefficients are stronger. In addition, it reduces the angular domain Ω, where VV is significantly below HH. Thus, if we consider a difference of at least 10 dB between these two coefficients to define Ω, we obtain the following width for this domain: 19° reduces to 18° when $\varepsilon_{\mathrm{r}2} = 10$ (see Fig. 2) is changed to $\varepsilon_{\mathrm{r}2} = 10 - \mathrm{j}\,3$ (see Fig. 3) and 22° reduces to 4° when $\varepsilon_{\mathrm{r}2} = 2.4$ is changed to $\varepsilon_{\mathrm{r}2} = 2.4 - \mathrm{j}\,4.5$. This decrease strongly depends on the permittivities.

When these permittivities are complex, we can no longer analytically determine the Brewster angle: we do not have a null R_{v} coefficient any more, and we can neither invoke the Snell–Descartes law. However, this case has already been studied in optics. Azzam and Ugbo define a pseudo-Brewster angle θ_{PB} that minimizes $|R_{\mathrm{v}}(\theta)|$ [2]. The angle θ_{PB} is determined using the quantity $u = \sin^2\theta_{\mathrm{PB}}$, solution to the following equation:

$$\left(2\varepsilon_{r_2} + 2|\varepsilon_{r_2}|^2\right)u^3 + \left(2|\varepsilon_{r_2}|^4 - 3|\varepsilon_{r_2}|^2\right)u^2 - 2|\varepsilon_{r_2}|^4 u + |\varepsilon_{r_2}|^4 = 0 \tag{7}$$

Numerically, we obtain $\theta_{\mathrm{PB}} = 65.1$ degrees for the first value $(\varepsilon_{\mathrm{r}2})$ and $\theta_{\mathrm{PB}} = 72.8$ degrees for the second case $(\varepsilon_{\mathrm{r}3})$. These values are totally consistent with the loci of the minimum for R_{v} observed in Fig. 3. We propose an empirical definition of θ_{PB} by extending Eq. (3) as follows:

$$\tilde{\theta}_{\mathrm{PB}} \simeq \arctan\sqrt{|\varepsilon_{r_2}|} \tag{8}$$

We calculated the relative error obtained between θ_{PB} and $\tilde{\theta}_{\mathrm{PB}}$ for permittivities, whose real and imaginary parts range in $[1, 50] \times [0, 50]$. We obtained an error less than to 5%, confirming the relevance of this approximation.

The direct link between the value of θ_{B} and θ_{PB} and the dielectric properties of the materials made it a good candidate for permittivity retrieval. In its simple form, the Brewster effect can only be observed in the specific specular configuration. However, most of radar data collections are monostatic, which implies that only the backscattering direction is observed. For that reason, we introduced in the next section what we called the *Double Brewster angle effect*, which is a physical phenomenon linked to the pseudo angle that can be observed in the monostatic configuration.

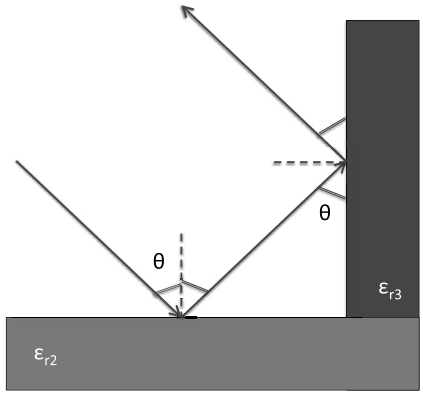

Fig. 4. The double-bounce on orthogonal faces of different complex permittivities ε_{r2} and ε_{r3}.

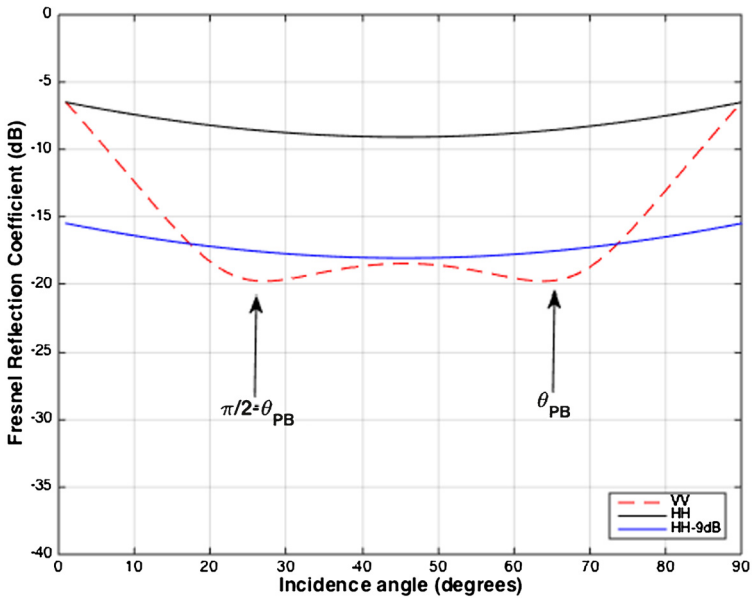

Fig. 5. Simulation of two successive reflection coefficients with $\varepsilon_{r_2} = \varepsilon_{r_3} = 2.4 - j4.5$: their variation with the incidence angle is plotted with black plain lines for $10\log_{10}(|R_h|^2)$ and in red dashed lines for $10\log_{10}(|R_v|^2)$. The blue line indicates HH–9dB.

3. The double Brewster angle effect

3.1. Definition and examples

We call the Double Brewster angle Effect (DBE) the combination of two successive specular reflections, that could lead to two pseudo Brewster angles: the first one linked to the horizontal interface and the second one associated with the vertical interface. This case is illustrated in Fig. 4, using a dihedral-type structure.

Indeed, a dihedral is made of two orthogonal faces, so its response in monostatic configuration can be simulated by the combination of two successive specular reflections. We consider that this dihedral is made of two lossy dielectrics ε_{r_2} and ε_{r_3}. In the first case, these materials are the same. As shown in Fig. 5, the first reflection occurs at θ_{PB}, while the second reflection happens at the complementary angle: $\pi/2 - \theta_{PB}$. As a consequence, there are two successive Brewster angles, the first one at θ_{PB} and the second one at the complementary angle $\pi/2 - \theta_{PB}$ as the second surface is rotated by $\pi/2$. This leads to a double Brewster effect spread over a wider range of incidence angles. For instance, in Fig. 5, R_v is 9 dB lower than R_h from 18 to 74 degrees for the incidence angle. In a second example, we consider a dihedral made of two different materials: $\varepsilon_{r2} = 2.4 - j4.5$ for the horizontal face and $\varepsilon_{r3} = 10. - j3$ for the vertical one. Fig. 6 shows that the two minima are now different and not localized at complementary angles. However, their angular positions are still obtained using Eq. (8). For this example, R_v is about 9 dB lower than R_h from 10 to 73 degrees for the incidence angle.

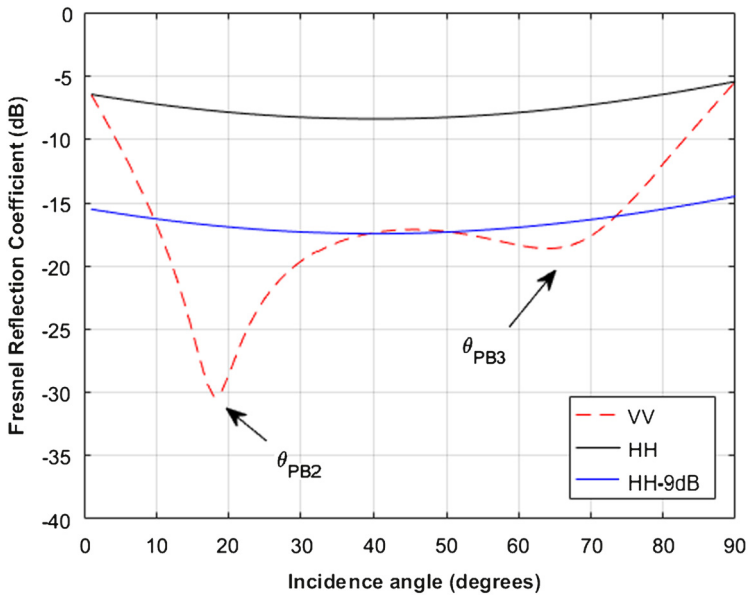

Fig. 6. Same as Fig. 5 but with $\varepsilon_{r_2} = 2.4 - j4.5$ while $\varepsilon_{r_3} = 10. - j3$.

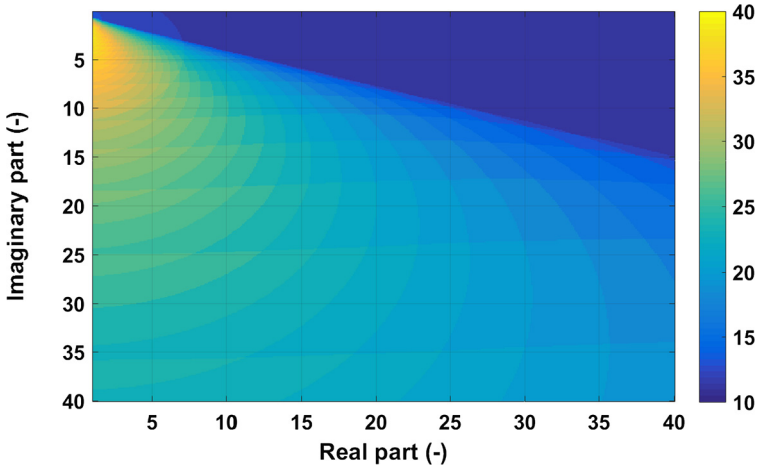

Fig. 7. The color indicates the width of the angle range (in degrees) where R_v is more than 10 dB lower than R_h for various real and imaginary parts of the permittivity of the vertical face. The permittivity of the horizontal face is kept constant and equal to $\varepsilon_{r2} = 32.3 - j16.9$. This corresponds to the permittivity of the ground of a tropical forest at P-band [8].

3.2. *Effect of the permittivity*

To generalize the previous results, we propose to keep the same configuration as the one proposed in the section before, except that ε_{r_3} is no more constant. Figs. 7 and 8 both show the width of the angular sector where the difference between R_v and R_h is larger than 10 dB as a function of the real and the imaginary parts of ε_{r_3}. For Fig. 7, we plot a forested situation, the permittivity of the horizontal part of the dihedral is the one of the ground for a tropical forest illuminated at P-band (see the forests described in [8]). For Fig. 8, we plot an urban case, the ground is made of concrete and observed at Ka-band [9]. We considered these two typical configurations to illustrate distinct situations and we used the same scale to compare them. However, this does not reflect neither the minimum nor the maximum that can be reached: for the concrete case, the largest width is equal to 65 degrees, while the smallest one measures 20 degrees; for the tropical ground, these widths are about 47 degrees and 11 degrees.

For the latter, the widest angular domains are obtained for the lowest values of the real part and for low values of the imaginary part. This angular domain can be very wide, up to 40° for the forest and up to 60° for the concrete. A difference of 10 dB between the two components means that the power of VV is at least 10 times lower than the power of HH. In other words, for many incidence angles, VV can be neglected with respect to HH. This effect is clearly stronger for the "urban" case that for "forested" configurations.

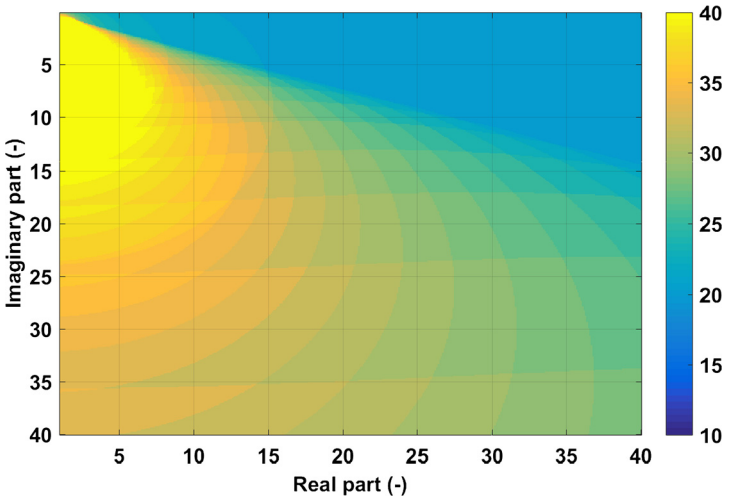

Fig. 8. The color indicates the width of the angle range (in degrees) where R_v is more than 10 dB lower than R_h for various real and imaginary parts of the permittivity of the vertical face. The permittivity of the horizontal face is kept constant and equal to $\varepsilon_{r2} = 10 - j3$. This is the permittivity for concrete at Ka-band [9].

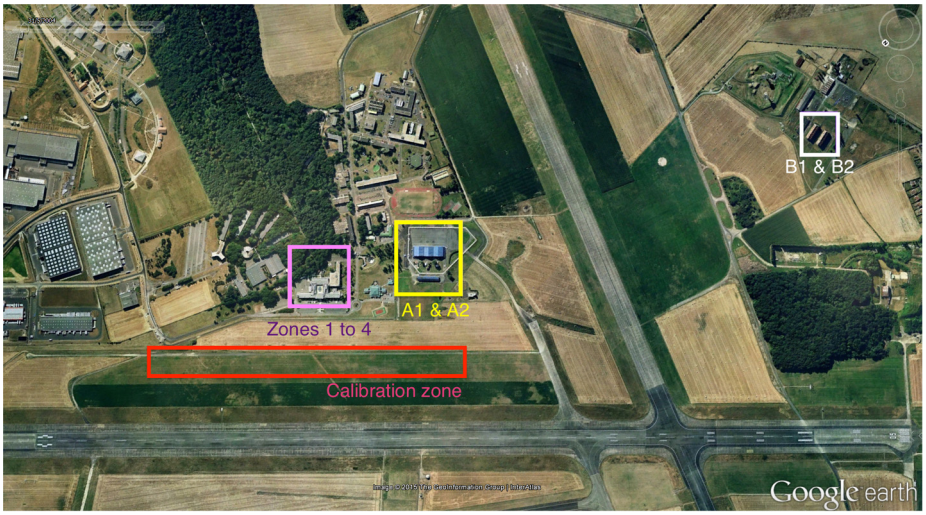

Fig. 9. Google Earth image of the area under study, taken on 01/05/2004. Corner reflectors have been put within the red rectangle for calibration purposes: four trihedrals and one rotated dihedral (45°). The pink, yellow, and white rectangles contain buildings of interest: their walls are made of dielectric materials. The top border of the forested stand below the white rectangle will be also studied.

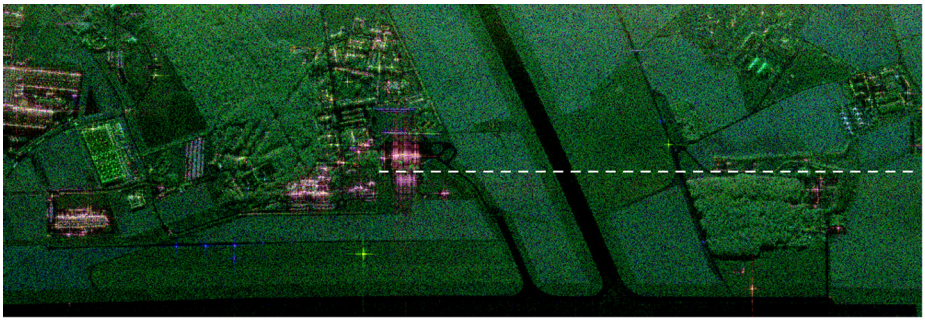

Fig. 10. PolSAR image acquired by ONERA (RAMSES) at X-band (1.32 m resolution along the range axis and 1.38 m along the azimuth axis) in the Pauli basis: $|VV - HH|$ in red, $|VV + HH|$ in blue and $|2HV|$ in green. The white dotted line indicates the location of the cut illustrated in Fig. 12.

Table 1
Measured backscattering cross sections (dBm^2) of the trihedrals and the dihedral located within the red rectangle.

	T1	T2	T3	T4	D1
HH	34.3	37.7	34.3	36.8	36.3
VV	34.1	38.1	34	36.6	36.4
VH	−2.4	0.7	−2.7	−5.4	37.7

4. Validation and illustration with real data

We saw in the previous section that a 10-dB difference minimum could be observed between VV and HH polarizations for two different configurations of permittivities. This large difference could actually be observed when two successive bounces occurred between two orthogonal plates composed of lossy dielectric materials. This difference can be obtained for a quite wide range of incidence angles, because we mix effects occurring at two complementary incidence angles: the one associated with the ground occurs between 45° and 90°, while the other linked to the vertical plate is in $[0°, 45°]$. For that reason, we expect to observe this effect on any polarimetric SAR image, provided that double bounces occur. We consider thus polarimetric airborne data with high resolutions (1.32 m along the range line and 1.38 m along the azimuth direction) at X-band and over a suburb area, mix of agricultural lands, forests and buildings. An optical view of this area is presented in Fig. 9. These data were acquired by ONERA with RAMSES sensor some 20 years ago over the French Air Force base of Bretigny-sur-Orge, at around 40 km south of Paris. A SAR image of this area is presented in Fig. 10 in the Pauli basis (VV−HH, VV+HH, HV+VH) [10]. The size of the illuminated area is about 1 km along the range axis and 2.5 km along the azimuth axis. Using this basis and our conventions, we recall that the intensity of (VV−HH) is a measure of the strength of the double bounces. The sensor trajectory was parallel to the main runway of the Air Force base and the radar illuminates the scene from the top to the bottom of the image.

4.1. The corner reflectors and the calibration

At the north of this runway, and parallel to it, four metallic trihedrals (T1 to T4) and one rotated dihedral (D1, 45°) have been aligned for calibration purposes (within the red rectangle in Fig. 9). These dihedrals are ideal references to check VV and HH amplitudes on this image. As expected, their amplitudes are equal, with a maximum difference of 0.4 dB between VV and HH values as illustrated in Table 1. We can then assume that the polarimetric calibration is good.

4.2. Validation on buildings

We then select buildings next to the calibration zone, all with dielectric walls:

A) in pink rectangle, one building made of dielectric material (with windows) and a variety of ground, cf. Fig. 11;
B) in the yellow rectangle, two buildings made of dielectric materials and parallel to the sensor path (A1 and A2), cf. Fig. 9;
C) in the white rectangle, two garrison buildings made of red bricks and rotated (30°) with respect to the sensor path (B1 and B2), cf. Fig. 9.

For each of these buildings, we computed the following quantity, reported in Table 2:

$$\Delta_{\mathrm{CoPol}} = 20\log_{10}\left(\langle|HH|\rangle - \langle|VV|\rangle\right) \tag{9}$$

We have also verified that these difference values are meaningful, in the sense that they are associated with strong signals, also reported in Table 2.

For the building in the pink zone, we have defined four zones of interest, as highlighted in Fig. 11. For all these zones, the wall is roughly the same, concrete with some windows. These are thus typical facades. The ground can however be different and zone 3 has some shadow due to the forest. Zone 1 and 4 have the largest difference Δ_{CoPol} (around 14–15 dB) between the copolarized signal. This was expected as the ground in front of these zones is made of bitumen. Zone 2 has a significant difference Δ_{CoPol} (about 10 dB), but smaller compared to zone 1 and 4 as the ground is a mix of bitumen and grass. For zone 3, Δ_{CoPol} is lower and varies significantly. The ground at that location is made of grass (so lower reflection) or a mix of grass and bitumen; some parts are probably shadowed by the forest.

For the two buildings (A1 and A2) in the yellow rectangle, the average has been computed along their longest dimension; we also observe strong differences between the two co-polarizations, up to 12 dB in average. All these buildings (zones 1 to 4 and A1 and A2) are aligned with the sensor path, so they exhibit double bounces and show a strong difference in Δ_{CoPol}, as predicted by the double Brewster angle effect. We did additional tests (not reported here); they all confirmed the difference between the co-polarization for dielectric buildings correctly oriented (so exhibiting a strong double bounce).

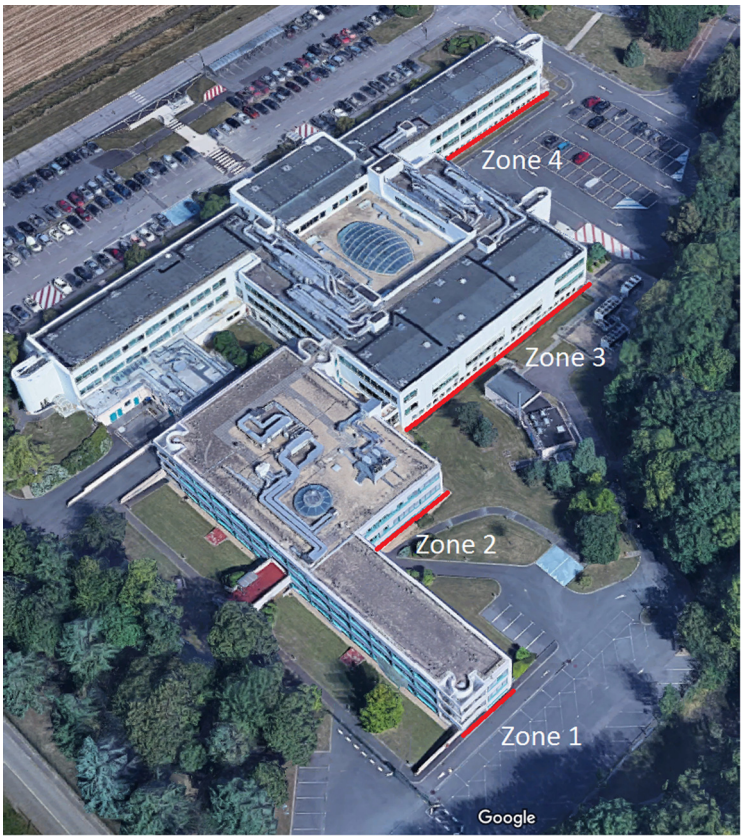

Fig. 11. Optical image of the building in the pink rectangle with the zone of interest.

Table 2
Measured values of Δ_{CoPol} (dBm^2) for the buildings within the pink (zones 1 to 4), yellow (A) and white (B) rectangles.

	Zone 1	Zone 2	Zone 3	Zone 4	A1	A2	B1	B2
Δ_{CoPol}	13.7	10.3	5–8	15.47	8.5	12	0	0
Hh	25.3	17.5	8.6–15.2	36.9				
Vv	11.5	7.2	4.3–7.3	21.4				

Considering buildings B1 and B2, which are also made of dielectric material, there is no difference between the co-polarizations. As these buildings are strongly rotated with respect to the sensor path, there is no more a dominant double bounce mechanism. As a consequence, there is no DBE. So we can observe that DBE disappears with rotation.

Finally, we checked the quantity Δ_{CoPol} for a metallic fence; we obtained 1.1 dB.

4.3. The border of forests

We finally propose a cut at range 441 (see Fig. 12). We test two quantities: first, the amplitude of the polarimetric double bounces calculated using $\langle |HH - VV| \rangle$ and plotted in dB in dashed red in Fig. 12; then, the differences between the amplitudes of the copolarizations ($|HH| - |VV|$ in dB) represented with black lines in Fig. 12.

Only the values above 0 dB have been plotted to better exhibit the cases of interest. We observe first that a difference exists between the two co-polarizations provided that the test on double-bounces is true. This has been noticed on the previous examples (buildings A1, A2, and zones 1 to 4). As the DBE results from a combination of two successive specular reflections on dielectric materials, it is mandatory to observe double bounces to see a DBE. On the contrary, when the test on double bounces is true, this does not systematically imply that there is a difference between the amplitudes of the copolarized channels. For metallic dihedrals, no significant differences exist between VV and HH amplitudes; however, these are strong double bounce returns.

In Fig. 12, at azimuth 800, we can see building A2 with its strong double bounce and its strong difference between the co-polarization, as described in the previous paragraph. Around azimuth 1200, there is the runway (no double bounce at all).

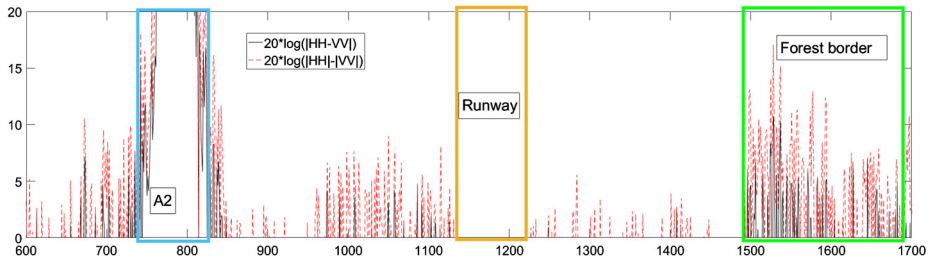

Fig. 12. Variation of the intensity along the range cut represented by a white dotted line in Fig. 10; from cell 600 to cell 1700, the distance is about 1.24 km. In red, we test the value of the Pauli component for the double bounces: $|HH - VV|$ in dB; in black, we plot $|HH| - |VV|$ in dB. The border of the forest begins at azimuth cell 1500 and is 207 m long.

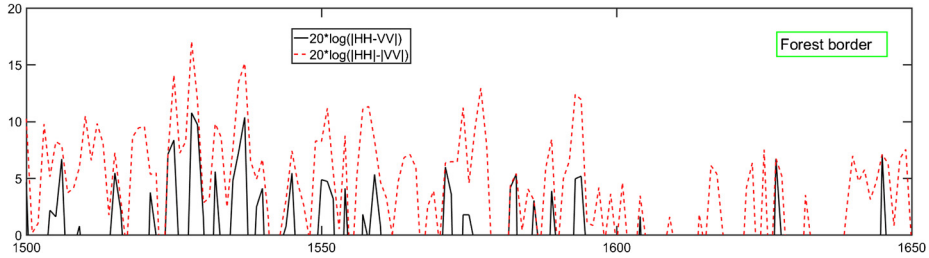

Fig. 13. Zoom on the forest part of Fig. 12. From cell 1500 to cell 1650, the distance is about 207 m. In red we test the value of Pauli component for the double bounces: $|HH - VV|$ in dB; in black, we plot $|HH| - |VV|$ in dB.

We now focus on the border of the forested areas, after azimuth 1500. This zoom is available in Fig. 13.

On this cut, the signature of forest starts at azimuth 1500. As the border is roughly parallel to the radar path and as it faces the aperture of the antenna, strong double bounces occur (up to 17dB at azimuth 1528). The values of $|HH| - |VV|$ varies along this border: from the almost null case to 11 dB (again at azimuth 1528) with lots of intermediate values around 5 dB. In particular, there are several azimuths with both strong double bounce and strong difference between the co-polarization, for instance at 1506, 1515, 1525, 1528, 1532, 1537, etc. This is highly probably due to double bounce mechanisms between trunks and the ground.

5. Conclusion

We recalled in this paper the definition of the Brewster angle for real permittivities and the pseudo-Brewster angle for complex ones. We then defined the double Brewster angle effect (DBE), which results from the combination of two pseudo-Brewster angles occurring in complementary incidence angles domains. As a result, this DBE can be observed for a large range of incidence angles, provided that the double bounce mechanism is present. We propose a simple model of DBE and we showed that the resulting reflection coefficients at VV and HH polarizations present a difference superior to 10 dB over a wide range of incidence angles – typically from 20 to 70°. This result occurs for a quite wide range of permittivities and therefore should be seriously considered, in urban or forested areas, for any application where double bounces can occur (radar, radio etc.). These findings have been tested on a polarimetric SAR image. Metallic trihedrals and a metallic dihedral used for calibration purposes at the time of the data acquisition have been considered to check the accuracy of the differences between HH and VV amplitudes measured on this image (less than 0.4 dB). On several well-oriented buildings with dielectric walls, we obtained a mean difference varying between 8 and 15 dB.

This DBE is sensitive to orientation, as it relies on the existence of double bounce. So we checked that it disappears for obliquely oriented buildings. Borders of forests have also been considered, and we saw differences that reached up to 11 dB between the two copolarized components.

We expect that this difference between VV and HH amplitudes can be sufficiently strong to seriously disturb some polarimetric analyses and, for instance, to create artefacts. This difference may constitute a reliable information on the material of hidden facades, which could help for security investigation. Then a major consequence is expected: the polarimetric signature can be dramatically affected in a way that has not been taken into account by the existing polarimetric tools. The interpretation of the radar and interferometric observations of land surfaces are then possibly biased; this can obviously affect the choice of the polarization modes proposed by the future systems.

Finally, this DBE phenomenon occurs over a wide range of incidence angles and for a broad frequency spectrum. It is likely to be observed by several systems on-board satellites, particularly by the forthcoming BIOMASS satellite (P-band). This could be also the case for communication systems operating in urban areas, for instance [11]. Therefore it would be of great interest to undertake as from now further and precise studies in order to detect this phenomenon, and the conditions of its occurring. This would underline the fact that usually the available data have already been pre-processed, a fact that could

bias or falsify some results. It is therefore of prime importance to have access to at least part of the original polarimetric data, before any pre-processing.

References

[1] D. Brewster, On the laws which regulate the polarisation of light by reflection from transparent bodies, Philos. Trans. R. Soc. Lond. 105 (1815) 125–159.
[2] R.M.A. Azzam, E.E. Ugbo, Contours of constant pseudo-Brewster angle in the complex ϵ plane and an analytical method for the determination of optical constants, Appl. Opt. 28 (24) (1989) 5222–5228, https://doi.org/10.1364/AO.28.005222, http://ao.osa.org/abstract.cfm?URI=ao-28-24-5222.
[3] A. Lakhtakia, Would Brewster recognize today's Brewster angle?, Opt. News 15 (6) (1989) 14–18.
[4] A. Fresnel, Mémoire sur la double réfraction, in: Oeuvre complète d'Augustin Fresnel, vol. 1, Imprimerie impériale, Paris, 1866.
[5] F.T. Ulaby, M.A. El-Rayes, Microwaves dielectric spectrum of vegetation. Part II: dual-dispersion model, IEEE Trans. Geosci. Remote Sens. 25 (5) (1987) 550–557.
[6] M. Hallikainen, F. Ulaby, M. Dobson, M. El-Rayes, L. Wu, Microwave dielectric behavior of wet soil. Part I: empirical models and experimental observations, IEEE Trans. Geosci. Remote Sens. 23 (1985) 25–34.
[7] A.I. Lvovsky, Fresnel equations, Ch. 63, pp. 1–6, http://www.tandfonline.com/doi/pdf/10.1081/E-EOE-120047133, https://doi.org/10.1081/E-EOE-120047133, http://www.tandfonline.com/doi/abs/10.1081/E-EOE-120047133.
[8] L. Thirion, E. Colin, C. Dahon, Capabilities of a forest coherent scattering model applied to radiometry, interferometry, and polarimetry at P- and L-band, IEEE Trans. Geosci. Remote Sens. 44 (4) (2006) 849–862.
[9] A. Mokadem, Analysis of Scattering by Urban Areas in the Frame of NLOS Target Detection in SAR Images, Ph.D. Thesis Graduate school STITS, University Paris 11, prepared at Supélec, Gif-sur-Yvette, France, February 2014, https://tel.archives-ouvertes.fr/tel-01080230/document.
[10] J.-S. Lee, E. Pottier, Polarimetric Radar Imaging: From Basics to Applications, CRC Press, Boca Raton, FL, USA, 2009.
[11] ITU-R, Future Technology Trends of Terrestrial IMT Systems, Recommendation M.2320, International Telecommunication Union, Geneva, 2015.